Functionalization of UiO-66 Metal-Organic Framework and Highly Cross-Linked Polystyrene with Cr(CO)(3): In Situ Formation, Stability, and Photoreactivity

UNIVERSITÀ DEGLI STUDI DI TORINO

Functionalization of UiO-66 metal-organic framework and highly cross-linked polystyrene with $Cr(CO)_3$: in situ formation, stability, and photo-reactivity

Sachin Chavan, Jenny G. Vitillo, Mohammed J. Uddin, Francesca Bonino, Carlo Lamberti, Elena Groppo, Karl-Petter Lillerud, Silvia Bordiga*

***This is an author version of the contribution published on**:*
Chem. Mater. 2010, 22, 4602–4611, DOI:10.1021/cm1005899

The definitive version is available at:
http://pubs.acs.org/doi/abs/10.1021/cm1005899

Functionalization of UiO-66 metal-organic framework and highly cross-linked polystyrene with $Cr(CO)_3$: *in situ* formation, stability, and photo-reactivity

Sachin Chavan,[1] Jenny G. Vitillo,[†] Mohammed J. Uddin,[†,2] Francesca Bonino,[†] Carlo Lamberti,[†] Elena Groppo,[†]* Karl-Petter Lillerud,[3] Silvia Bordiga[†]

E-mail: elena.groppo@unito.it

Department of Inorganic, Physical and Material Chemistry, University of Torino, via Giuria 7, 10125 Torino, and NIS Centre of Excellence and INSTM Centro di Riferimento, via Quarello 11, I-10135, Torino (Italy), inGAP Centre of Research-Based Innovation Department of Chemistry, University of Oslo, P.O. Box 1033, N-0315 Oslo, Norway

Abstract

The formation and stability of (arene)$Cr(CO)_3$ species inside two highly porous materials - UiO-66, a recently synthesized metal-organic framework, and a cross-linked poly(styrene-co-divinylbenzene) resin - is investigated in details by means of complementary spectroscopic techniques and theoretical calculations. In particular, FT-IR, UV-Vis and XANES spectroscopies, coupled with theoretical calculations, allow to follow *in situ* the formation of the (arene)$Cr(CO)_3$ species starting from the $Cr(CO)_6$ precursor, monitoring the changes in the vibrational and electronic properties of the materials. EXAFS spectroscopy gives the structural evidence of the functionalizing unities. Finally, the photo-induced reactivity of $Cr(CO)_3$ in UiO-66 is also explored, by following the substitution of one CO ligand with a N_2 molecule. The overall presented data would become the starting point for the development of a systematic procedure for investigating functionalized porous matrices.

[1] University of Torino
[2] Present address: Department of Chemical Engineering & Polymer Science, Shah Jalal University of Science & Technology, SUST, Sylhet-3114, Bangladesh.
[3] University of Oslo

1. Introduction

Functionalization of metal-organic framework (MOF) materials remains one of the main challenges driving the MOF community,[1-9] even more than the optimization of the synthesis conditions to make always newer and newer structures. Indeed, the metal sites in most of the MOFs structures show at maximum one coordination vacancy (and only after removal of the solvent), therefore limiting their application *e.g.* in catalysis, where at least two coordination vacancies are required. The post-synthesis introduction of metal moieties in the framework by grafting is one of the strategies followed in the perspective of application of MOF in catalysis.[4-6,10-20] Grafting of metal containing species can occur when the MOF framework shows reacting groups (such as –OH, –NH, and others); however, this excludes the application of the method in case of MOFs that do not have functional groups (or have in very small amount). Another possibility is the direct functionalization of the arene belonging to the organic linkers. Indeed, there exist several examples of organometallic species where the metal site is coordinated to a π-donor arene ring. This strategy has been followed recently by Kaye and Long[21] who successfully functionalized MOF-5 by grafting $Cr(CO)_3$ units on the benzene ring of the organic linker; and by Kamegawa et al.[22] who reported the functionalization of an inorganic-organic hybrid mesoporous silica with the same species. In both cases, the functionalization proceeded through thermal decomposition of $Cr(CO)_6$ precursor, following the reaction reported in Scheme 1.

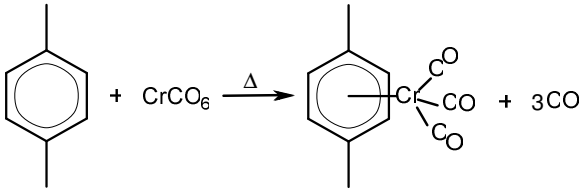

Scheme 1. Schematic representation of the thermal decomposition of $Cr(CO)_6$ in presence of an arene moiety, with consequent formation of (η^6-arene)$Cr(CO)_3$ species, followed by release of CO.

The (η^6-arene)$Cr(CO)_3$ species are particularly interesting because they play important roles in heterogeneous catalysis (*e.g.* hydrogenation of polyunsaturates into cis-unsaturated products) and are building blocks in organometallic chemistry.[23,24] Moreover, $M(CO)_n$ units have been found to substitute at least one CO ligand with one N_2 or H_2 under UV light irradiation (following the reaction shown in Scheme 2),[25-29] a behavior that opens interesting perspectives in the field of the storage of small molecules.

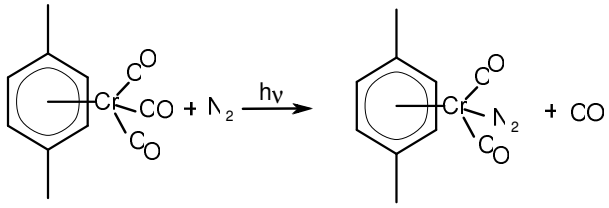

Scheme 2. Schematic representation of the UV-induced CO substitution by N_2 ligand for (η^6-arene)$Cr(CO)_3$ species, with attendant release of CO.

As a consequence of these first (rapid) communications, many efforts have been devoted to the theoretical estimation of the stability and reactivity of $Cr(CO)_3$ species grafted on benzene rings as a function of the electron-donor or electron-acceptor nature of the ring substituent.[30-33] Very recently, some of us has demonstrated that there exists a relation between the stability of the grafted (η^6-arene)$Cr(CO)_3$ adducts and experimentally valuable quantities, as obtained by XRD and XAS and FT-IR spectroscopies.[34]

In the present work, we report on the functionalization of the recently synthesized UiO-66 material with $Cr(CO)_3$ moieties. UiO-66 is a cubic close packed three-dimensional metal-organic framework composed by a zirconia based inorganic building brick and 1,4-benzene dicarboxylic

acid (H_2BDC) as organic linker;[35] the Zr sites do not present any coordination vacancy. For this reason, the obtained results can be directly compared with those obtained by functionalizing a completely organic material, *i.e.* a poly(styrene-co-divinylbenzene) resin (hereafter PS). Despite its amorphous nature, the PS matrix presents a very high surface area and a porosity very similar to those displayed by the UiO-66 material, which are achieved through a high cross-linking degree. Therefore, it offers a good opportunity to evaluate experimentally the influence of the ring substituent on the structural, electronic and vibrational properties of the grafted $Cr(CO)_3$. The formation, reversibility and stability of the two systems are systematically investigated by FT-IR, UV-Vis, XANES and EXAFS spectroscopies, complemented by quantum mechanical calculations. Moreover, the photo-induced reactivity of $Cr(CO)_3$ in UiO-66 is also explored, by following the substitution of one CO ligand with a N_2 molecule. Finally, complementary results obtained in case of the similar $Mo(CO)_3$ grafted species are reported in the Supporting Information, with the aim to show the role of the metal in affecting the investigated properties.

Even if the possibility to functionalize hybrid organic/inorganic structures by means of $M(CO)_n$ species has been already reported in the past,[21,22] the occurrence of a similar reactivity in case of completely organic matrices (such as PS) has never been shown. Moreover, a complete vibrational, electronic and (especially) structural characterization by means of several spectroscopic techniques coupled with theoretical calculations is still missing. The present work has the ambitious goal to completely describe the functionalization of two categories of porous materials (metal-organic frameworks and cross-linked polymers) by means of an organometallic approach, and would like to become the starting point for the development of a systematic procedure of investigation of functionalized porous matrices.

2. Materials and methods

2.1 Materials

UiO-66. $Zr_6O_4(OH)_4(CO_2)_{12}$ is a cubic close packed 3D metal-organic framework composed by a zirconia based inorganic building brick and 1,4-benzene dicarboxylic acid (H_2BDC) as a organic linker. The details of the structure and synthesis have been reported elsewhere.[35] In the typical synthesis, a mixture of $ZrCl_4$ and H_2BDC in NN'-dimethyl formamide is heated in sealed oven at 120°C for 24 h. The material, stable up to 350°C, crystallized as small (0.2 μm) intergrown cubic crystals. UiO-66 has a Langmuir surface area of 1187 m^2g^{-1} and pores with opening ranging from 6 to 10 Å.

PS. The cross-linked polymer used in these experiments is a poly(styrene-co-divinylbenzene) resin commercialized by Aldrich in the form of 300–800 μm beads. The polymer presents a BET surface area of 1000 m^2g^{-1}, as evaluated by N_2 adsorption measurement at 77 K, and a pore size distribution centered around 16 Å.[36] The permanent open texture characterising this porous polymeric matrix is obtained by 25% cross linking level with divinylbenzene, and allows the easy diffusion of molecules from the gas phase.

$Cr(CO)_6$ and $(\eta^6\text{-}C_6H_6)Cr(CO)_3$ were obtained from Strem Chemicals Co. and Aldrich, respectively, and used without any treatment.

In situ formation of the (arene)$M(CO)_3$ species. Prior to the dosage of metal hexacarbonyls, both UiO-66 and PS have been activated in vacuum in order to remove all the adsorbates (solvents and water), each one at the proper experimental conditions, *i.e.* at 250°C (for 30 min) and at room temperature (for 60 min), respectively. $M(CO)_6$ (M = Cr or Mo) was then dosed from the gas phase upon vacuum sublimation of the solid at room temperature. Finally, the matrices were treated in presence of $M(CO)_6$ at 150°C (i.e. below the decomposition temperature of $Cr(CO)_6$) in order to

optimize the formation of the (arene)$M(CO)_3$ species (see section 3.1). The stability of both $M(CO)_6$ precursor and of the $M(CO)_3$ products is different in the two matrices, as will be discussed in the following.

2.2. Methods

Experimental. FTIR spectra were collected in transmission mode at 2 cm^{-1} resolution on a Bruker IFS66 spectrophotometer equipped with both MCT and DTGS detectors. The experiments have been performed either on self supporting pellets and thin depositions on silicon, as described previously.[37] For $Cr(CO)_6$ and $(C_6H_6)Cr(CO)_3$ in THF solution, the IR measurements were performed in a cell for liquids. Parallel DR-UV-Vis-NIR measurements were performed on a Cary 5000 spectrometer equipped with a reflectance sphere on thick self-supported pellets. In all experiments samples were put inside ad hoc cells that allow thermal treatments in high vacuum conditions, dosage of probe molecules and *in situ* spectra collection to be performed.

X-ray absorption experiments at the Cr K-edge (5989 eV) were performed at the BM26A beamline (DUBBLE) of the ESRF facility (Grenoble, F). The white beam was monochromatized using a Si(111) double crystal; harmonic rejection has been performed by using a meridionally focusing mirror with an angle of incidence of 2.8 mrad and a silicon coating. The spectra of the (η^6-C_6H_6)$Cr(CO)_3$ and $Cr(CO)_6$ reference samples have been collected in transmission mode, on self supporting pellets diluted with boron nitride. Conversely, in the case of PS/$Cr(CO)_3$, due to the chromium dilution, EXAFS spectra were collected in fluorescence mode, by means of a 9 elements germanium monolithic detector. To avoid contamination, the sample was sealed in a glass capillary (1.5 mm in diameter), following the well established procedure adopted for XRPD experiments.[38] For this reason, the beam was vertically focused in order to reach a dimension on the sample of 0.3 mm. The horizontal slits were optimized to fit with the interval of uniform filling of the capillary. This procedure, which is common in XRPD measurements, is not standard for EXAFS measurements, because requires a very stable beam along the whole energy scan. We have successfully applied this strategy in previous cases.[39]

The XANES part of the spectra was acquired with an energy step of 0.4 eV and an integration time of 2 s/point. The EXAFS part of the spectra was collected up to 12 $Å^{-1}$ with a variable sampling step in energy, resulting in $\Delta k = 0.05$ $Å^{-1}$, and an integration time that linearly increases as a function of k from 5 to 20 s/point to account for the low signal-to-noise ratio at high k values. For each sample, three equivalent EXAFS spectra were acquired and averaged before the data analysis.[40] EXAFS data analysis was performed using the Arthemis software,[41] following the strategy reported in details in SI.

Theoretical Calculations. The calculations have been performed with the *Gaussian 03* software package[42] at the B3LYP level of calculation.[43,44] The UiO-66 framework has been modeled by means of benzene and *p*-$C_6H_4(COOH)_2$. These cluster models have been successfully used to reproduce the CO vibrational shifts of grafted $Cr(CO)_3$ species on MOFs in Ref. [34]. For the hydrogen atoms, the standard Pople basis set supplemented by diffuse and polarizability functions 6-311++G(2d,2p) has been adopted.[45,46] For all the other elements, the fully optimized triple-ζ valence basis sets proposed by Ahlrichs *et al.*[47] have been used, augmented by two sets of polarization functions derived from the original ones following an even-tempered recipe that is by substituting the polarization orbital in the basis set with two orbitals, having respectively the coefficient doubled and halved with respect to the parent orbital. The so obtained basis sets will be indicated as TZV2p. Geometry optimization has been carried out by means of the Berny optimization algorithm with analytical gradient. No geometrical constraints have been imposed. For further details on the calculations please refer to Ref. [34].

Harmonic frequencies have been obtained by determining analytically the second derivatives of the energy with respect to the Cartesian nuclear coordinates and then transforming to mass-weighted coordinates. No scaling factor has been adopted.

The UV-Vis spectra were obtained from Time Dependent Density Functional Theory (TDDFT)[48,49] calculations for the (η^6-C_6H_6)$Cr(CO)_3$ and [η^6-$C_6H_4(COOH)_2$]$Cr(CO)_3$ complexes in the gas phase. TDDFT is well-known as a rigorous formalism for the treatment of excitation energies within the DFT. In particular it has been successfully applied in literature for the calculation of excitation energies of metal complexes.[32,50-52] A total of 100 singlet excited states and their corresponding oscillator strengths were determined. The theoretical spectrum was obtained through a Gaussian convolution of the peaks by using the Gauss View 4.1 Program. The electronic distribution and localization of the singlet excited states were visualized using electron density difference maps.

3. Results and Discussion

3.1. Formation and stability of (arene)$Cr(CO)_3$ complexes

3.1.1 Vibrational properties: in situ FT-IR spectroscopy

$Cr(CO)_6$ in the gas phase is characterized by four IR-active modes of T_{1u} symmetry:[53] CO stretching ν(CO), metal-carbon-oxygen bending δ(Cr-C-O), metal-carbon stretching ν(Cr-C) and carbon-metal-carbon deformation *def*(C-Cr-C), that give rise to four IR absorption bands centered at 2000, 668, 440 and 98 cm^{-1}, respectively. Due to instrumental limitations, only the ν(CO) and δ(Cr-C-O) regions were accessible and therefore only these two regions will be discussed in the following. When $Cr(CO)_6$ is dissolved in THF (dark grey curve in Figure 1b), its molecular symmetry is slightly perturbed. As a consequence, the IR absorption bands slightly shift in frequency (ν(CO) at 1979 cm^{-1} and δ(Cr-C-O) at 665 cm^{-1}) and also the Raman active ν(CO) vibration of E_g symmetry becomes visible (weak band at 2020 cm^{-1}). A similar "solvent effect" is also observed when $Cr(CO)_6$ is adsorbed inside both PS and UiO-66 matrices (dark grey curves Figure 1c and d): the IR spectra are dominated by a very intense, out of scale, IR absorption band centered around 1980 cm^{-1} (IR-active mode) and by a weaker band around 2020 cm^{-1} (Raman active).[54] Similar bands have been reported in the past in case of $Cr(CO)_6$ adsorbed on oxides.[55-57] In the low frequency range, the band associated to δ(Cr-C-O) is observed around 664 cm^{-1} in both cases.

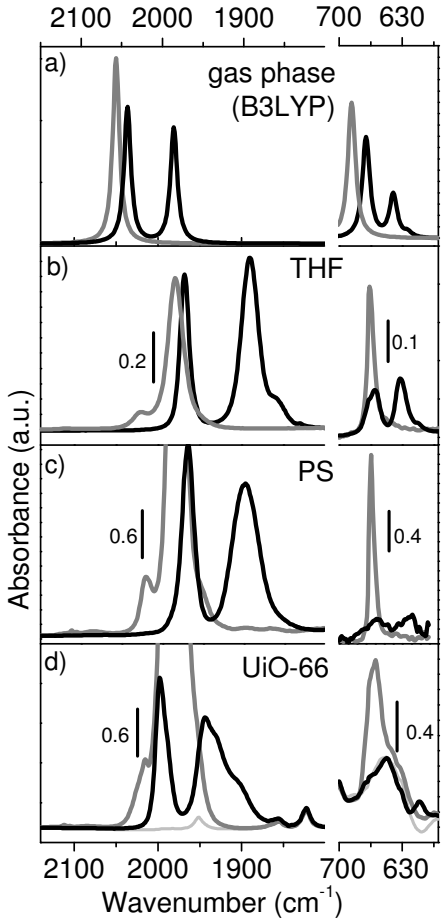

Figure 1. FTIR spectra of $Cr(CO)_6$ (dark grey) and (η^6-C_6H_6)$Cr(CO)_3$ (black) as obtained by B3LYP calculation (part a, unscaled spectra), and experimentally determined in THF (part b), and in PS and UiO-66 supports (parts c and d). Left and right parts display the ν(CO) and δ(Cr-C-O) regions, respectively. In parts b-c background subtracted spectra are reported, whereas in part d the spectrum of the UiO-66 is reported in light grey.

Even though the vibrational features of $Cr(CO)_6$ physisorbed in PS and UiO-66 are very similar, the two systems show strong difference in their stability upon evacuation. In particular, in case of PS the adsorbed $Cr(CO)_6$ is completely removed by outgassing at room temperature, whereas in case of UiO-66, $Cr(CO)_6$ is almost irreversibly adsorbed at room temperature, and it can be removed only upon prolonged outgassing at 150°C. This is in agreement with what is expected on electrostatic basis.[34] Due to this difference, the thermal decomposition of $Cr(CO)_6$ was performed following two different procedures: (i) by heating at 150°C for 12 h in closed cell, followed by outgassing at room temperature, in the case of PS; (ii) by heating at 150°C for 12 h in dynamic vacuum, in the case of UiO-66. After the thermal treatment, both samples become colored (light and dark yellow, respectively, vide infra the UV-Vis spectra in Section 3.1.2), suggesting the formation of (arene)$Cr(CO)_3$ species. Indeed, the FT-IR spectra obtained after the thermal decomposition of $Cr(CO)_6$ are dominated by two new IR absorption bands in the ν(CO) region (black curves in Figure 1c and d), at a lower frequency with respect to the $Cr(CO)_6$ bands. These two bands, very similar to those observed in case of (η^6-C_6H_6)$Cr(CO)_3$ in THF (black curve in Figure 1b), are easily assigned to the non-degenerate total symmetric stretching $\nu(CO_{totsym})$ and to the doubly degenerate total asymmetric stretching $\nu(CO_{asym})$ of the (arene)$Cr(CO)_3$ species.[53] A qualitative picture of the bonding in transition metal π-complexes involves a donation of charge from the arene to the metal and then, in turn, from the metal to the carbonyl groups, which results into an increase of the strength of the Cr-CO bond as compared with $Cr(CO)_6$ and into a decrease of the C-O bond strength as compared with $Cr(CO)_6$ and CO.[34,58] This explains why the vibrational

modes of the (arene)$Cr(CO)_3$ species are at lower frequency with respect to those of $Cr(CO)_6$. In the low frequency range, the disappearance of the sharp component around 664 cm^{-1} testifies the absence of unreacted $Cr(CO)_6$, while the attendant appearance of weak bands in the δ(Cr-C-O) region, at 659 and 620 cm^{-1} for PS/$Cr(CO)_3$ and at 610 cm^{-1} for UiO-66/$Cr(CO)_3$, is associated with the formation of (arene)$Cr(CO)_3$ species (compare the same region for (η^6-C_6H_6)$Cr(CO)_3$ in THF, Figure 1b). It is worth noticing that, the changes observed in the experimental spectra before and after the thermal treatment correspond to the difference in the computed spectra of $Cr(CO)_6$ and(η^6-C_6H_6)$Cr(CO)_3$, respectively (unscaled, Figure 1a).

Entering in more details, the PS/$Cr(CO)_3$ system (black spectrum in Figure 1c) shows a narrow IR absorption band at 1966 cm^{-1} and a broader one at 1898 cm^{-1}, very close to those of (η^6-C_6H_6)$Cr(CO)_3$ in THF (black curve in Figure 1b), whereas the same bands appear at 1998 and 1944 cm^{-1} respectively, in the case of UiO-66/$Cr(CO)_3$ system (black curve in Figure 1d). The blue-shift of the ν(CO) bands in the case of UiO-66/$Cr(CO)_3$ can be explained by considering the electron-accepting nature of the arene substituent, as recently demonstrated by Vitillo et al.[34] Basically, an electron-accepting substituent on the ring (such as the carboxylate of the UiO-66 matrix) decreases the charge transfer to the metal and further decreases the Cr-CO bond order, while at the same time increases the C-O bond order as compared with the unsubstituted complex.

Beside the different frequency position, the two IR absorption bands characterizing PS/$Cr(CO)_3$ and UiO-66/$Cr(CO)_3$ have a larger full-width at half-maximum (fwhm) with respect to the pure (η^6-C_6H_6)$Cr(CO)_3$, even if the relative ratio of the fwhm's of the two bands is the same. This evidence suggests a higher heterogeneity of the grafted species in the two investigated supports. Moreover, in the case of UiO-66/$Cr(CO)_3$ system the band centered at 1944 cm^{-1} is constituted by at least three different components (at 1943, 1929 and 1904 cm^{-1}), a fact that can be explained by considering $Cr(CO)_3$ moieties feeling a slightly different environment. Indeed, the local environment of a $Cr(CO)_3$ species in UiO-66 is quite complex. UiO-66 is characterized by two type of cages, a tetrahedral one (smaller) and a hexahedral one (larger), accounting for half of the volume each and with the same entrance windows, as reported in Figure 2 (dotted grey lines). Due to the steric encumbrance, only one $Cr(CO)_3$ species can be hosted in the tetrahedral cage, whereas two functionalities can found place in the hexahedral one, provided that they are formed on two opposite benzene rings. From the graphical representation reported in Figure 2 is clear that the carbonyl species are surrounded by a different environment in the two type of cages; this is likely the origin of the slightly different vibrational properties highlighted by FT-IR spectroscopy. Finally, it is worth noticing that the structure of UiO-66 is completely retained after the functionalization, as demonstrated by XRPD data (collected in controlled atmosphere, see Figure S1).

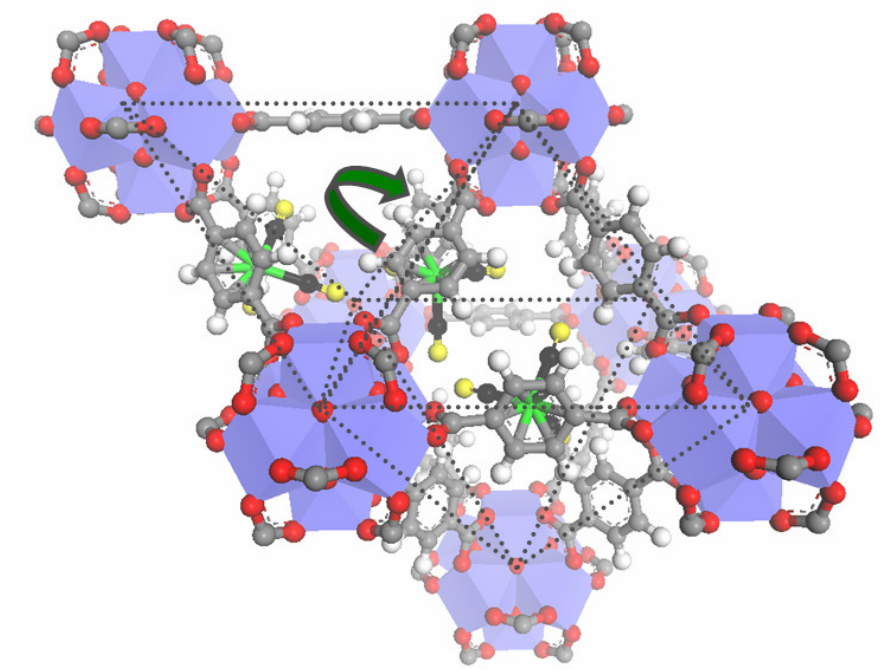

Figure 2. Graphic representation of (arene)$Cr(CO)_3$ species formed inside UiO-66; the tetrahedral and hexahedral cages are emphasized by dotted grey lines. The Zr atoms are represented as blue octahedra with O (red) at the corners; C and H atoms are shown in grey and white, respectively. Cr, C and O of the $Cr(CO)_3$ moieties are reported in green, dark grey and yellow, respectively. The green arrow illustrates that a rotation by 45° of the benzene ring will move the $Cr(CO)_3$ from one cage to the neighboring cage.

The so formed (arene)$Cr(CO)_3$ species are pretty stable in presence of CO (at least for few hours), *i.e.* they are not converted back to $Cr(CO)_6$. This is evident in Figure 3a, as no changes in the FT-IR spectra of the (arene)$Cr(CO)_3$ complexes are observed when 40 mbar of CO are dosed at room temperature. Conversely, the formed complexes are less stable in presence of air/moisture (Figure 3b). The stability is greater when the complexes are formed in a hydrophobic matrix (PS) with respect to much hydrophilic one (UiO-66). The stability of the corresponding (arene)$Mo(CO)_3$ complexes in UiO-66 and PS has been characterized also, and the results are reported in the SI. As a general statement, the stability of (arene)$M(CO)_3$, both in presence of CO and of air/moisture, follows the order Cr > Mo. As shown in SI, a considerable formation of $Mo(CO)_6$ species in presence of CO is observed, whereas upon exposure to moisture the complexes are nearly complete decomposed (Figure S3).

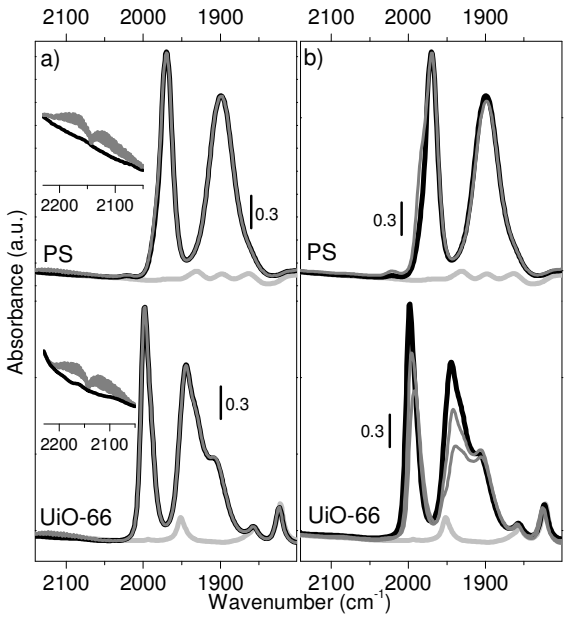

Figure 3. Reversibility in presence of CO (part a) and stability in air (part b) of the (arene)$Cr(CO)_3$ species formed in PS (top) and in UiO-66 (bottom). Light grey: background; black: (arene)$Cr(CO)_3$; dark grey: evolution upon CO dosage or exposure to air. Insets in part a show a magnification of the 2250-2030 cm^{-1}, where the rotovibrational profile of gaseous CO is present.

3.1.2 Optical properties: in situ DR UV-Vis-NIR spectroscopy

As already anticipated in the previous section, upon heating the PS and UiO-66 matrices in presence of $Cr(CO)_6$ the samples became colored, pale and dark yellow in the two cases, respectively, in close analogy to the bright yellow color of the (η^6-C_6H_6)$Cr(CO)_3$ reference compound. The UV-Vis spectrum of (η^6-C_6H_6)$Cr(CO)_3$ in ethanol solution (dotted curve in top part of Figure 4a) shows a well defined band centered around 32000 cm^{-1}. The spectrum of solid (η^6-C_6H_6)$Cr(CO)_3$ (diluted in silica, dashed curve in top part of Figure 4a) displays also a shoulder at about 26500 cm^{-1}. Theoretical calculations assign these absorption bands to a charge-transfer from the $Cr(CO)_3$ fragment to the benzene ring, in agreement with literature.[32,58] The simulated optical spectrum for (η^6-C_6H_6)$Cr(CO)_3$ in gas phase is displayed in Figure 4b (dotted curve), together with a graphical representation of the corrisponding electronic transitions (electron density moves from orange orbitals to the blue ones). It is worth noticing that two transitions are predicted at around 35000 (band A) and 29000 cm^{-1} (band B), the second one almost forbidden. Transitions implying an electron density movement from the (η^6-C_6H_6)Cr moiety to the carbonyl ligands occur at higher frequencies, and are not considered in this work.

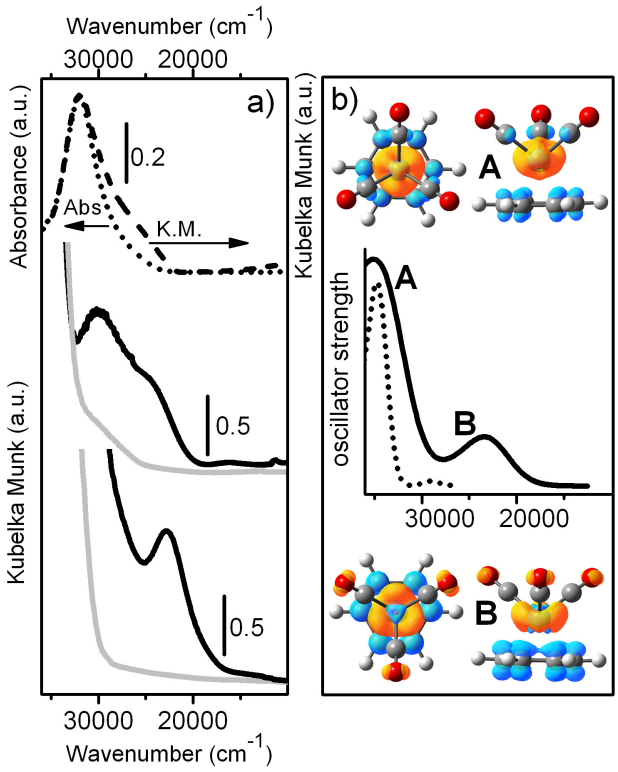

Figure 4. Part a): experimental UV-Vis spectra of the (arene)$Cr(CO)_3$ species. Top part: bare (η^6-C_6H_6)$Cr(CO)_3$ sample in the solid state (diluted in silica, in DR mode, dashed curve) and in ethanol solution (in transmission mode, dotted curve). Middle and bottom parts: (arene)$Cr(CO)_3$ formed inside PS and in UiO-66 samples, respectively (black curves). Grey curves refer to the spectra of the corresponding empty supports. Part b): TDDFT optical spectra of (C_6H_6)$Cr(CO)_3$ and (p-C_6H_4)$(COOH)_2Cr(CO)_3$ (dotted and full lines, respectively). Top and bottom parts display the difference in the electron density of the states involved in the A and B electronic transitions (blue, positive values; orange, negative values).

Similar bands in the visible region are observed in the case of the (arene)$Cr(CO)_3$ species formed inside PS and UiO-66 matrices, as reported in central and bottom part of Figure 4a (full black curves). In both cases, the intense absorption band with an edge at around 30000 cm^{-1} is assigned to the π–π* transition of the arene moieties characterizing the matrices (compare the spectra with those of the corresponding pure matrices, grey curves). Beside this feature, the spectrum of the PS/$Cr(CO)_3$ system shows a complex band centered around 28000 cm^{-1} with two components at 30000 and 25000 cm^{-1}. For UiO-66/$Cr(CO)_3$, the optical spectrum displays an intense, out of scale, band around 30000 cm^{-1} and a well defined one at 23000 cm^{-1}. In close analogy with (η^6-C_6H_6)$Cr(CO)_3$, these absorption bands are associated with $(CO)_3Cr \rightarrow$ arene charge-transfer transitions. We expect that the different electron-donor nature of the arene substituent should affect the frequency position of the two components. By comparing the results of calculations performed on (p-C_6H_4)$(COOH)_2Cr(CO)_3$ with those of (C_6H_6)$Cr(CO)_3$ (dotted and full lines in Figure 4b), it is clear that the presence of the carboxylate substituent strongly affect the electronic transitions. In particular, it causes a bathochromic shift of band B, that shifts from 29100 to 23400 cm^{-1}, and an increase of its intensity with respect to band A. This is in fine agreement with the experimental results and nicely explains why the spectrum of UiO-66/$Cr(CO)_3$ shows a more intense, better resolved, band at lower frequency with respect to the spectrum of PS/$Cr(CO)_3$.

3.1.3 Structural and electronic properties of PS/$Cr(CO)_3$ investigated by XAS spectroscopy

Both FTIR and UV-Vis spectroscopies give strong evidence of formation of (arene)$Cr(CO)_3$ species inside the PS and UiO-66 matrices. In order to have a structural confirmation of the nature of the formed species, XAS spectroscopy was performed on the PS/$Cr(CO)_3$ sample. This is a lucky case, since the matrix is highly transparent to the X-ray, and therefore it is possible to get a reasonable signal to noise ratio also in highly diluted conditions. It is worth underlining that these data give the first structural evidence of formation of (arene)$Cr(CO)_3$ species inside a porous matrix. This is also much more important by considering that it is obtained in the case of an amorphous matrix, where XRPD measurements are not informative. Indeed, EXAFS spectroscopy is extremely powerful in defining the local environment around the absorbing atom, independently from the presence of a long range order. Unfortunately, EXAFS was not possible in the case of UiO-66/$Cr(CO)_3$ system, at least in our experimental conditions, because the matrix is highly absorbing at the Cr K-edge energy due to the presence of Zr atoms.

The XANES spectrum of the PS/$Cr(CO)_3$ sample is shown in Figure 5a (black curve), and compared to the spectra of the (η^6-C_6H_6)$Cr(CO)_3$ and $Cr(CO)_6$ references sample (light grey and dark grey, respectively). All the spectra contain several pre-edge features (A) below the first (B, well defined peak at 6006 eV) and the second (C, broad component around 6025 eV) strong resonances. Resonance B has the highest intensity in each spectrum. The presence of a sharp (A) resonance, followed at about 20 eV by a broader one (B) is typical of the XANES spectra of linear metal carbonyl complexes.[59,60] However, it is well known that the intensity ratio between resonance B and the shape resonance C varies as a function of the number of CO ligands: when going from the octahedral $Cr(CO)_6$ to the pseudo-tetrahedral (η^6-C_6H_6)$Cr(CO)_3$, resonance B becomes weaker and resonance C is broadened.[61] Therefore, in a first approximation it is possible to deduce the number of carbonyl ligands characterizing the species formed in the PS matrix by looking at the relative ratio between the two resonances. Additionally, the intensity of the pre-edge features increases by going from perfect octahedral complexes to pseudo-tetrahedral ones. Indeed, the pre-edge features are assigned to the $A_{1g}\rightarrow T_{2g}$ and $A_{1g}\rightarrow E_g$ transitions, which are dipole-forbidden in a perfect octahedral case, but become allowed when the symmetry is lowered.[40,62,63] Coming in more details, $Cr(CO)_6$ presents two weak pre-edge bands at 5993 and 5997 eV, whereas (η^6-C_6H_6)$Cr(CO)_3$ is characterized by a sharp and quite intense band at 5991 eV with a shoulder at 5993 eV, and by a weaker component at 5996 eV, which appears overlapped to the sharp white line feature. It is evident that a careful comparison of the pre-edge region could give important information on the local structure around Cr in the complex formed inside PS.

The XANES spectrum of the PS/$Cr(CO)_3$ sample is very similar to that of the (η^6-C_6H_6)$Cr(CO)_3$ reference, as evidenced especially by the derivative signal (bottom part in Figure 5a), with the following exceptions: (i) unless at the same energy position, the pre-edge features are less intense; (ii) feature B is less intense; (iii) the shape resonance C is slightly different. These features suggest that the complexes formed inside PS are characterized by a coordination geometry slightly different with respect to the bare complex in the solid state. In particular, it has been pointed out that resonance C contains information on the bond length between Cr and C atoms of the carbonyl ligands.[61] A change in this region suggests therefore a difference in the geometry of the carbonyl ligands around Cr by going from (η^6-C_6H_6)$Cr(CO)_3$ to PS/$Cr(CO)_3$. These differences, qualitatively predicted from XANES spectra, will be quantitatively estimated by fitting the EXAFS data.

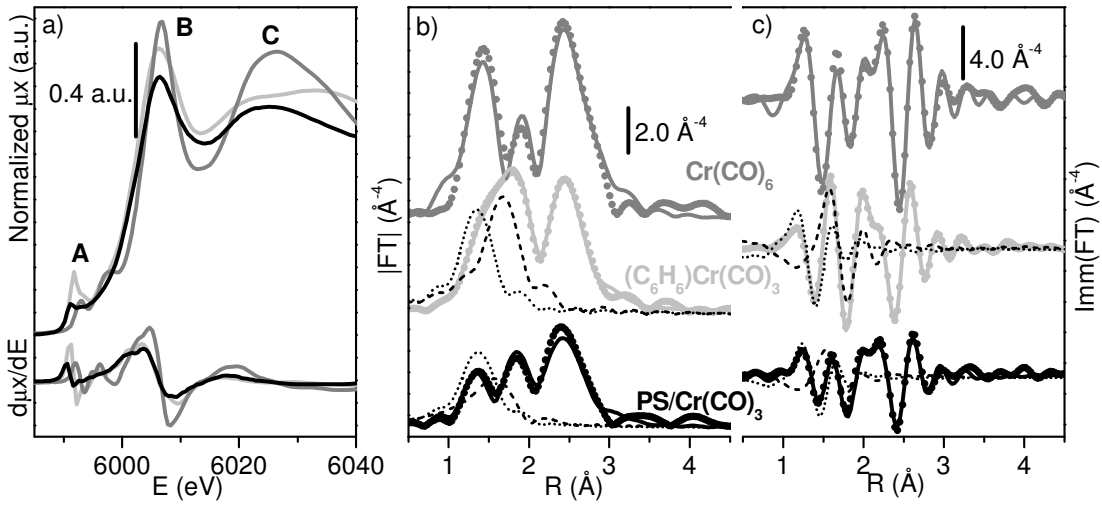

Figure 5. Part a: XANES spectra of PS/$Cr(CO)_3$ species (black), compared to those of the (η^6-C_6H_6)$Cr(CO)_3$ (light grey) and $Cr(CO)_6$ (grey) reference compounds. Both the normalized μx and the derivative spectra are reported (top and bottom parts, respectively). Parts b and c: k^3-weighted, phase uncorrected, FT of the EXAFS spectra of PS/$Cr(CO)_3$ species (bottom), compared to those of the (η^6-C_6H_6)$Cr(CO)_3$ (middle) and $Cr(CO)_6$ (top) reference compounds. in modulus and imaginary parts, respectively. The experimental data (scattered circles) are compared with the best fits (full line). In case of PS/$Cr(CO)_3$ and (η^6-C_6H_6)$Cr(CO)_3$, dotted and dashed curves are the first shell SS contributions due to Cr-C_{CO} and Cr-C_{Bz} respectively, as estimated by the best fit.

The k^3-weighted, phase uncorrected, FT of the EXAFS functions for PS/$Cr(CO)_3$ is reported in Figure 5b,c in both modulus and imaginary parts, and compared to those of the reference compounds. Clear differences in the coordination shell of Cr are observed. The |FT| of $Cr(CO)_6$ (top part of Figure 5b) is dominated by two peaks, centered at 1.4 and 2.4 Å (without phase correction), which correspond to the first shell Cr-C and second shell Cr-O contributions of the six carbonyl ligands, respectively. Note that the second shell peak is very high in intensity due to the important contributions of the collinear Cr-C-O MS paths, enhanced by focusing effect. The results of the data analysis (see first column in Table 1 and full line in top part of Figure 5b,c) are in agreement with the structural data obtained by XRD.[59,60,64] A completely different signal is obtained in the case of (η^6-C_6H_6)$Cr(CO)_3$ (middle part of Figure 5b,c). In this case the |FT| is still dominated by two main components but, while the second one occurs almost at the same position of that found for $Cr(CO)_6$, the first one is clearly doubled and shifted in distance. This is due to the fact that the first coordination shell around Cr is composed by three carbonyl ligands (dotted curve) and six carbon atoms belonging to the benzene ring (dashed curve), at a slightly different distance (see second column in Table 1). This results into an apparent shift of the first shell component towards higher distances with respect to the $Cr(CO)_6$ sample.

As far as PS/$Cr(CO)_3$ is considered, the |FT| spectrum (bottom part of Figure 5b) is completely different from the spectra of both the reference compounds, being characterized by three peaks, the first two with an overall intensity which is around half of that shown by the first shell signal of both $Cr(CO)_6$ and (η^6-C_6H_6)$Cr(CO)_3$. Actually, the three peaks arise from the combination of the two first shell signals coming from the CO ligands (dotted curve) and the benzene ring (dashed curve), respectively. In this case, both the Cr-C_{Bz} and Cr-C_{CO} distances are slighlty modified with respect to the (η^6-C_6H_6)$Cr(CO)_3$ reference compound, so that they are now almost opposite in phase (see imaginary parts in bottom part of Figure 5c). This phenomenon is the main responsible for the decrease in intensity of the overall signal (since a part of the signal is cancelled by the negative interpherence between the first shell signals). The data analysis results into 2.7 ± 0.6 carbonyl ligands at an average distance ($R_{Cr\text{-}CO}$) of 1.88 ± 0.01 Å, and 5.4 ± 1.2 carbons of the arene ring at

an average distance (R_{Cr-Bz}) of 2.220 ± 0.006 Å (see third column in Table 1). The Debye-Waller factor obtained for the arene ligand (0.016 ± 0.005 $Å^2$) is indicative of a certain degree of heterogeneity; this is expected, since the arene rings belong to the flexible and heterogeneous PS matrix. Notwithstanding the small differences in the relative distance of Cr with respect to the CO and arene ligands, EXAFS spectroscopy definitely proves, also from a structural point of view, that the species formed inside PS are of the type (arene)$Cr(CO)_3$. The small geometrical differences and the higher heterogeneity (Debye-Waller values) with respect to the structure of the bare compound in the solid state could be responsible of the differences observed in the UV-Vis spectra between the PS/$Cr(CO)_3$ sample and (η^6-C_6H_6)$Cr(CO)_3$ reference compound.

Table 1. Summary of the structural parameters optimized in the fit of the EXAFS data for the PS/$Cr(CO)_3$ sample and for the (η^6-C_6H_6)$Cr(CO)_3$ and $Cr(CO)_6$ reference compounds: structural factor (S_0^2); edge-energy (ΔE_0), number of carbonyls (N_{CO}) and of C atoms belonging to the benzene ring (N_{Bz}); average distance between Cr and the C atoms of carbonyls (R_{Cr-CO}) and between Cr and the C atoms of benzene rings (R_{Cr-Bz}); Debye-Waller factors (σ^2_{CO} and σ^2_{Bz}). The fits run in R-space, in the 1.0-3.2 Å range, over a k^3-weighted FT of the $\chi(k)$ functions performed in the 2.0-11.0 $Å^{-1}$ interval. A single S_0^2 and a single ΔE_0 have been optimized for all SS and MS paths. Not optimized parameters are recognizable by the absence of the corresponding error bars.

	$Cr(CO)_6$	(η^6-C_6H_6)$Cr(CO)_3$	PS/$Cr(CO)_3$
S_0^2	0.8 ± 0.1	1.0 ± 0.1	1
ΔE_0 (eV)	-2 ± 1	-2 ± 1	-4 ± 1
N_{CO}	6	3	2.7 ± 0.6
R_{Cr-CO} (Å)	1.908 ± 0.008	1.850 ± 0.004	1.88 ± 0.01
σ^2_{CO} ($Å^2$)	0.004 ± 0.001	0.0054 ± 0.0007	0.006 ± 0.002
N_{Bz}	-	6	5.4 ± 1.2
R_{Cr-Bz} (Å)	-	2.220 ± 0.006	2.20 ± 0.03
σ^2_{Bz} ($Å^2$)	-	0.006 ± 0.001	0.014 ± 0.005
R_{factor}	0.042	0.007	0.042

3.1. Photoreaction of UiO-66/$Cr(CO)_3$

Photochemistry of organometallic (η^6–arene)$M(CO)_3$ complexes has been extensively studied in solution,[25,65] matrix isolation,[32,66] super critical fluid,[27] and polymeric matrices.[22,28] Photoactive organometallic compounds adsorbed or supported on high surface area porous supports could serve as important gas storage media (in particular H_2)[67] and also as active catalyst sites (photocatalytic hydrogenation of dienes)[68-70] if present in sufficient concentration, well dispersed, and in chemically accessible form. Depending upon the photolysis condition, one or more CO can be removed, to produce coordinatively unsaturated metal sub-carbonyls or even metal atoms.[66,71-74] Moreover, it has been also demonstrated that such systems undergo light activated substitution chemistry, in which CO ligand is replaced by N_2 and H_2.[27,29,66,75] Recently, Kaye et al.[21] have shown that the $Cr(CO)_3$ moieties anchored on benzene ring of MOF-5 undergo analogous photochemical reaction when irradiated with a 450 nm laser.

Here we made a similar attempt on UiO-66. After functionalization, UiO-66/$Cr(CO)_3$ has been exposed to UV light in N_2 atmosphere for increasing time. The occurrence of light activated substitution of one CO ligand with a N_2 molecule has been followed by both FT-IR and UV-Vis spectroscopies (Figure 6). Few minutes of UV irradiation are sufficient to cause relevant modifications in both FT-IR and UV-Vis spectra. In the FT-IR spectra (Figure 6a), the two bands centered at 1998 and 1944 cm^{-1} characterizing the (arene)$Cr(CO)_3$ species (black spectrum) decrease in intensity, with the attendant formation of a weak and broad band at 2187 cm^{-1} (red spectrum), which is easily assigned to ν(NN) of coordinated N_2, demonstrating the formation of the

mixed complex UiO-66/$Cr(CO)_2(N_2)$. In addition, a small absorption appears in the region between the main ν(CO) bands, accompanied by a shoulder around 1901 cm^{-1}. The obtained spectrum is very similar to that reported in literature for $Zn_4O[(BDC)Cr(CO)_2(N_2)]_3$[21] and for of $(C_6H_6)Cr(CO)_2(N_2)$,[27] and well agrees with the changes expected on the basis of theoretical calculations performed on two possible conformers of $C_6H_4(COOH)_2Cr(CO)_2N_2$ (Figure 6c). It is worth noticing that only a small fraction of $Cr(CO)_3$ are interested by the substitution, mainly because the experiment is conducted in static conditions.

Finally, exposure times longer than 30 minutes lead to the decomposition of the (arene)$Cr(CO)_3$ species, as testified by the disappearance of the vibrational bands in both ν(CO) and ν(NN) regions (spectra not reported). The same occurs on the PS/$Cr(CO)_3$ sample after very short irradiation time, suggesting a higher lability of the complex under UV irradiation (spectra not reported).

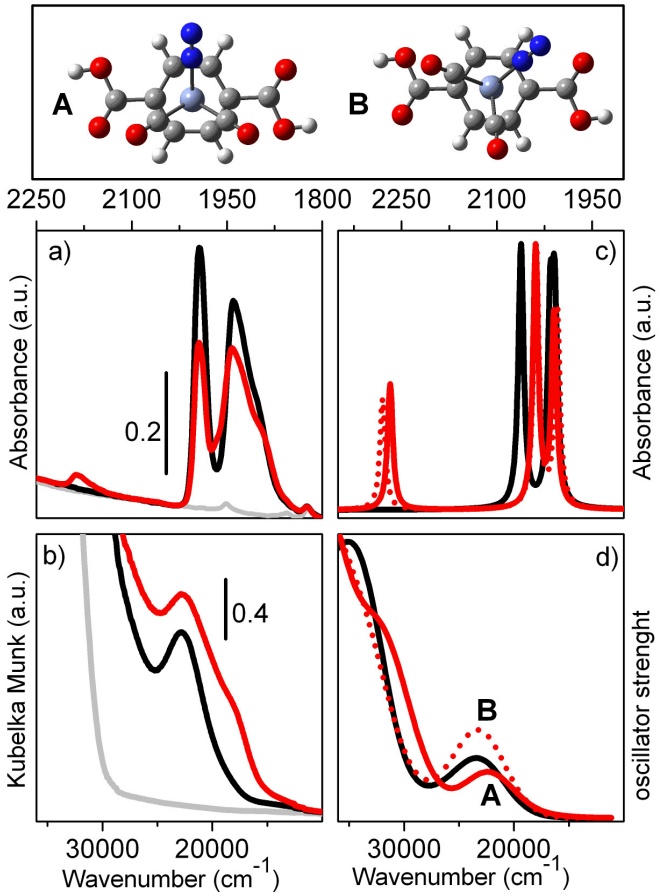

Figure 6. Part a) Evolution of the FT-IR spectrum of UiO-66/$Cr(CO)_3$ (black) upon photoirradiation under N_2 atmosphere (red) for 5 minutes. The spectrum of UiO-66 before functionalization is reported in grey. Part b): Same experiments followed by UV-Vis spectroscopy. Parts c) and d): Simulated IR and optical spectra for $(C_6H_4)(COOH)_2Cr(CO)_3$ (black) and for the two conformers of $(C_6H_4)(COOH)_2Cr(CO)_2(N_2)$ (full and dotted red lines for conformer A and B, respectively).

The light-activated CO substitution by N_2 in UiO-66/$Cr(CO)_3$ is also demonstrated by the changes in the UV-Vis spectrum (Figure 6b). After irradiation for few minutes, the sample slightly changes in color; as a consequence, the overall intensity of the UV-Vis spectrum increases and a new band at 18450 cm^{-1} appears. These changes are nicely predicted by theoretical calculations

performed on two possible conformers of $C_6H_4(COOH)_2Cr(CO)_2N_2$ (Figure 6d). In case of conformer A (full red line in Figure 6d), the simulated electronic transitions are red-shifted with respect to $C_6H_4(COOH)_2Cr(CO)_3$ (black line), whereas for conformer B an increase in intensity is observed (dotted red line). The experimental spectrum obtained for UiO-66/$Cr(CO)_2(N_2)$ can be explained in terms of co-presence of both conformers, thus explaining both the increase of the overall intensity and the appearance of a band at lower frequency with respect to the starting spectrum.

4. Conclusions

Two highly porous matrices (UiO-66 and PS), whose structure is characterized by the presence of differently substituted benzene rings, have been successfully functionalized by grafting $Cr(CO)_3$ species, following the thermal decomposition of $Cr(CO)_6$ precursor. UiO-66 is a cubic close packed three-dimensional metal-organic framework composed by a zirconia based inorganic building brick and 1,4-benzene dicarboxylic acid as organic linker, where the Zr sites do not present any coordination vacancy. PS is a commercial poly(ethyl-co-divinylbenzene), with a surface area and porosity very similar to those of UiO-66. The vibrational, electronic and structural properties of the grafted $Cr(CO)_3$ species have been completely investigated by means of FT-IR, UV-Vis, XANES and EXAFS spectroscopies, complemented by theoretical calculations. It is definitely demonstrated that the nature of the benzene ring substituent (a carboxylate or a CH_2 group, respectively) influences the final properties of the functionalized matrix, as previously predicted by theoretical calculation.[34] In case of UiO-66/$Cr(CO)_3$ material, also the photo-induced substitution of one CO ligand with a N_2 molecule under UV irradiation has been explored.

The functionalization of highly porous, hybrid or completely organic, matrices (either crystalline or amorphous in nature) with $Cr(CO)_3$ species opens interesting perspective in the field of heterogeneous catalysis, organometallic chemistry, as well as storage of small molecules. Therefore, the here reported data could be of interest for a wide scientific community, and suggest a systematic procedure to investigate the functionalization process of porous matrices.

Acknowledgements

Prof. A. Zecchina is kindly acknowledged for fruitful discussion. The whole staff of BM26 (and in particular S. Nikitenko) are gratefully acknowledged for the help provided during the XAS measurements. This work is part of the STREP Project MOFCAT contract number NMP4-CT-2006-033335.

Synopsis TOC

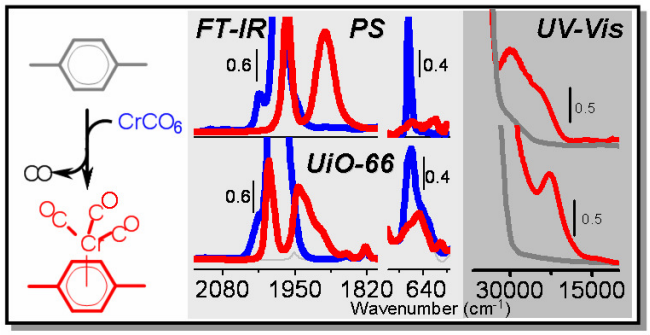

References and Notes

(1) Yamada, T.; Kitagawa, H. *J. Am. Chem. Soc.* 2009, *131*, 6312.
(2) Gadzikwa, T.; Farha, O. K.; Mulfort, K. L.; Hupp, J. T.; Nguyen, S. T. *Chem. Commun.* 2009, 3720.
(3) Gadzikwa, T.; Farha, O. K.; Malliakas, C. D.; Kanatzidis, M. G.; Hupp, J. T.; Nguyen, S. T. *J. Am. Chem. Soc.* 2009, *131*, 13613.
(4) Goto, Y.; Sato, H.; Shinkai, S.; Sada, K. *J. Am. Chem. Soc.* 2008, *130*, 14354.
(5) Qiu, S. L.; Zhu, G. S. *Coord. Chem. Rev.* 2009, *253*, 2891.
(6) Savonnet, M.; Aguado, S.; Ravon, U.; Bazer-Bachi, D.; Lecocq, V.; Bats, N.; Pinel, C.; Farrusseng, D. *Green Chem.* 2009, *11*, 1729.
(7) Ingleson, M. J.; Heck, R.; Gould, J. A.; Rosseinsky, M. J. *Inorg. Chem.* 2009, *48*, 9986.
(8) Hong, D. Y.; Hwang, Y. K.; Serre, C.; Ferey, G.; Chang, J. S. *Adv. Funct. Mater.* 2009, *19*, 1537.
(9) Tanabe, K. K.; Wang, Z. Q.; Cohen, S. M. *J. Am. Chem. Soc.* 2008, *130*, 8508.
(10) Das, S.; Kim, H.; Kim, K. *J. Am. Chem. Soc.* 2009, *131*, 3814.
(11) Gascon, J.; Aktay, U.; Hernandez-Alonso, M. D.; van Klink, G. P. M.; Kapteijn, F. *J. Catal.* 2009, *261*, 75.
(12) Jiang, D. M.; Urakawa, A.; Yulikov, M.; Mallat, T.; Jeschke, G.; Baiker, A. *Chem.-Eur. J.* 2009, *15*, 12255.
(13) Natarajan, S.; Mahata, P. *Chem. Soc. Rev.* 2009, *38*, 2304.
(14) Lee, J.; Farha, O. K.; Roberts, J.; Scheidt, K. A.; Nguyen, S. T.; Hupp, J. T. *Chem. Soc. Rev.* 2009, *38*, 1450.
(15) Shultz, A. M.; Farha, O. K.; Hupp, J. T.; Nguyen, S. T. *J. Am. Chem. Soc.* 2009, *131*, 4204.
(16) Nelson, A. P.; Farha, O. K.; Mulfort, K. L.; Hupp, J. T. *J. Am. Chem. Soc.* 2009, *131*, 458.
(17) Lu, Y.; Tonigold, M.; Bredenkotter, B.; Volkmer, D.; Hitzbleck, J.; Langstein, G. *Z. Anorg. Allg. Chem.* 2008, *634*, 2411.
(18) Proch, S.; Herrmannsdorfer, J.; Kempe, R.; Kern, C.; Jess, A.; Seyfarth, L.; Senker, J. *Chem.-Eur. J.* 2008, *14*, 8204.
(19) Ingleson, M. J.; Barrio, J. P.; Guilbaud, J. B.; Khimyak, Y. Z.; Rosseinsky, M. J. *Chem. Commun.* 2008, 2680.
(20) Wu, C. D.; Hu, A.; Zhang, L.; Lin, W. B. *J. Am. Chem. Soc.* 2005, *127*, 8940.
(21) Kaye, S. S.; Long, J. R. *J. Am. Chem. Soc.* 2008, *130*, 806.
(22) Kamegawa, T.; Sakai, T.; Matsuoka, M.; Anpo, M. *J. Am. Chem. Soc.* 2005, *127*, 16784.
(23) Rosillo, M.; Dominguez, G.; Perez-Castells, J. *Chem. Soc. Rev.* 2007, *36*, 1589.
(24) Gibson, S. E.; Ibrahim, H. *Chem. Commun.* 2002, 2465.
(25) Upmacis, R. K.; Poliakoff, M.; Turner, J. J. *J. Am. Chem. Soc.* 1986, *108*, 3645.
(26) Sweany, R. L. *J. Am. Chem. Soc.* 1985, *107*, 2374.
(27) Howdle, S. M.; Healy, M. A.; Poliakoff, M. *J. Am. Chem. Soc.* 1990, *112*, 4804.
(28) Goff, S. E. J.; Nolan, T. F.; George, M. W.; Poliakoff, M. *Organometallics* 1998, *17*, 2730.
(29) Zheng, Y.; Wang, W.; Lin, J.; She, Y.; Fu, K. *J. Phys. Chem.* 1992, *96*, 9821.
(30) Suresh, C. H.; Koga, N.; Gadre, S. R. *Organometallics* 2000, *19*, 3008.
(31) Lochan, R. C.; Khaliullin, R. Z.; Head-Gordon, M. *Inorg. Chem.* 2008, *47*, 4032.
(32) Alamiry, M. A. H.; Brennan, P.; Long, C.; Pryce, M. T. *J. Organomet. Chem.* 2008, *693*, 2907.
(33) Alamiry, M. A. H.; Boyle, N. M.; Brookes, C. M.; George, M. W.; Long, C.; Portius, P.; Pryce, M. T.; Ronayne, K. L.; Sun, X. Z.; Towrie, M.; Vuong, K. Q. *Organometallics* 2009, *28*, 1461.
(34) Vitillo, J. G.; Groppo, E.; Bordiga, S.; Chavan, S.; Ricchiardi, G.; Zecchina, A. *Inorg. Chem.* 2009, *48*, 5439.
(35) Cavka, J. H.; Jakobsen, S.; Olsbye, U.; Guillou, N.; Lamberti, C.; Bordiga, S.; Lillerud, K. P. *J. Am. Chem. Soc.* 2008, *130*, 13850.
(36) Spoto, G.; Vitillo, J. G.; Cocina, D.; Damin, A.; Bonino, F.; Zecchina, A. *Phys. Chem. Chem. Phys.* 2007, *9*, 4992.

(37) Chavan, S.; Bonino, F.; Vitillo, J. G.; Groppo, E.; Lamberti, C.; Dietzel, P. D. C.; Zecchina, A.; Bordiga, S. *Phys. Chem. Chem. Phys.* 2009.
(38) Palomino, G. T.; Bordiga, S.; Zecchina, A.; Marra, G. L.; Lamberti, C. *J. Phys. Chem. B* 2000, *104*, 8641.
(39) Estephane, J.; Groppo, E.; Damin, A.; Vitillo, J. G.; Gianolio, D.; Lamberti, C.; Bordiga, S.; Prestipino, C.; Nikitenko, S.; Quadrelli, E. A.; Taoufik, M.; Basset, J. M.; Zecchina, A. *J. Phys. Chem. C* 2009, *113*, 7305.
(40) Lamberti, C.; Bordiga, S.; Arduino, D.; Zecchina, A.; Geobaldo, F.; Spanò, G.; Genoni, F.; Petrini, G.; Carati, A.; Villain, F.; Vlaic, G. J. *J. Phys. Chem. B* 1998, *102*, 6382.
(41) Ravel, B.; Newville, M. *Phys. Scr.* 2005, *T115*, 1007.
(42) Gaussian 03.
(43) Becke, A. D. *J. Chem. Phys.* 1993, *98*, 5648.
(44) Lee, C.; Yang, W.; Parr, R. G. *Phys. Rev. B* 1988, *37*, 785.
(45) Clark, T.; Chandrasekhar, J.; Spitznagel, G. W.; Schleyer, P. v. R. *J. Comp. Chem.* 1983, *4*, 294.
(46) Frisch, M. J.; Pople, J. A.; Binkley, J. S. *J. Chem. Phys.* 1984, *80*, 3265.
(47) Schäfer, A.; Huber, C.; Ahlrichs, R. *J. Chem. Phys.* 1994, *100*, 5829.
(48) Casida, M. E.; Jamorski, C.; Casida, K. C.; Salahub, D. R. *J. Chem. Phys.* 1998, *108*, 4439.
(49) Stratmann, R. E.; Scuseria, G. E.; Frisch, M. J. *J. Chem. Phys.* 1998, *109*, 8218.
(50) Ciofini, I.; Laine, P. P.; Bedioui, F.; Adamo, C. *J. Am. Chem. Soc.* 2004, *126*, 10763.
(51) Salassa, L.; Garino, C.; Salassa, G.; Gobetto, R.; Nervi, C. *J. Am. Chem. Soc.* 2008, *130*, 9590.
(52) Vlček, A. *Coord. Chem. Rev.* 1998, *177*, 219.
(53) Adams, D. M., *Metal-Ligand and Related Vibrations*; Edward Arnold (Publisher) Ltd London: London, 1967.
(54) Note 01.
(55) Guglielminotti, E. *J. Mol. Catal.* 1981, *13*, 207.
(56) Platero, E. E.; Arean, C. O.; Scarano, D.; Spoto, G.; Zecchina, A. *Mater. Chem. Phys.* 1991, *29*, 347.
(57) Zecchina, A.; Arean, C. O. *Catal. Rev.-Sci. Eng.* 1993, *35*, 261.
(58) Carrol, D. G.; McGlykn, S. P. *Inorg. Chem.* 1968, *7*, 1285.
(59) Lamberti, C.; Palomino, G. T.; Bordiga, S.; Berlier, G.; D'Acapito, F.; Zecchina, A. *Angew. Chem. Int. Edit.* 2000, *39*, 2138.
(60) Prestipino, C.; Capello, L.; D'Acapito, F.; Lamberti, C. *Phys. Chem. Chem. Phys.* 2005, *7*, 1743.
(61) Engemann, C.; Hormes, J.; Longen, A.; Dotz, K. H. *Chem. Phys.* 1998, *237*, 471.
(62) Bordiga, S.; Coluccia, S.; Lamberti, C.; Marchese, L.; Zecchina, A.; Boscherini, F.; Buffa, F.; Genoni, F.; Leofanti, G.; Petrini, G.; Vlaic, G. *J. Phys. Chem.* 1994, *98*, 4125.
(63) Groppo, E.; Lamberti, C.; Spoto, G.; Bordiga, S.; Magnacca, G.; Zecchina, A. *J. Catal.* 2005, *236*, 233.
(64) Filipponi, A.; Dicicco, A.; Zanoni, R.; Bellatreccia, M.; Sessa, V.; Dossi, C.; Psaro, R. *Chem. Phys. Lett.* 1991, *184*, 485.
(65) Simon, J. D.; Xie, X. *J. Phys. Chem.* 1986, *90*, 6751.
(66) Bloyce, P. E.; Hooker, R. H.; Rest, A. J.; Bitterwolf, T. E.; Fitzpatrick, N. J.; Shade, J. E. *J. Chem. Soc.-Dalton Trans.* 1990, 833.
(67) Cooper, A. I.; Poliakoff, M. *Chem. Commun.* 2007, 2965.
(68) Clarke, M. J.; Cooper, A. I.; Howdle, S. M.; Poliakoff, M. *J. Am. Chem. Soc.* 2000, *122*, 2523.
(69) Jackson, S. A.; Hodges, P. M.; Poliakoff, M.; Turner, J. J.; Grevels, F. W. *J. Am. Chem. Soc.* 1990, *112*, 1221.
(70) Childs, G. I.; Cooper, A. I.; Nolan, T. F.; Carrott, M. J.; George, M. W.; Poliakoff, M. *J. Am. Chem. Soc.* 2001, *123*, 6857.
(71) Brecknridge, W. H.; N., S. *J. Phys. Chem.* 1981, *85*, 3557.

(72) Tumas, W.; Gitlin, B.; Rosan, A. M.; Yardley, J. T. *J. Am. Chem. Soc.* 1982, *140*, 55.
(73) Fletcher, T. R.; Rosenfeld, R. N. *J. Am. Chem. Soc.* 1983, *105*, 6358.
(74) Seder, T. A.; Church, S. P.; Ouderkirk, A. J.; Writz, E. *J. Am. Chem. Soc.* 1985, *107*, 1432.
(75) Walsh, E. F.; George, M. W.; Goff, S.; Nikiforov, S. M.; Popov, V. K.; Sun, X. Z.; Poliakoff, M. *J. Phys. Chem.* 1996, *100*, 19425.

Supporting information

Functionalization of UiO-66 metal-organic framework and highly cross-linked polystyrene with $Cr(CO)_3$:

in situ formation, stability, and photo-reactivity

Sachin Chavan,[4] Jenny G. Vitillo,[†] Mohammed J. Uddin,[†,5] Francesca Bonino,[†] Carlo Lamberti,[†] Elena Groppo,[†]* Karl-Petter Lillerud,[6] Silvia Bordiga[†]

E-mail: elena.groppo@unito.it

Department of Inorganic, Physical and Material Chemistry, University of Torino, via Giuria 7, 10125 Torino, and NIS Centre of Excellence and INSTM Centro di Riferimento, via Quarello 11, I-10135, Torino (Italy), inGAP Centre of Research-Based Innovation Department of Chemistry, University of Oslo, P.O. Box 1033, N-0315 Oslo, Norway

[4] University of Torino
[5] Present address: Department of Chemical Engineering & Polymer Science, Shah Jalal University of Science & Technology, SUST, Sylhet-3114, Bangladesh.
[6] University of Oslo

The (arene)$Cr(CO)_3$ complexes

Structural properties of UiO-66/$Cr(CO)_3$

XRPD measurements in controlled atmosphere (sealed capillaries) have been perfomed on both the UiO-66 matrix (dehydrated at 150°C) and the UiO-66/$Cr(CO)_3$ material. The patterns, reported in Figure S1, are almost equivalent, demonstrating that the functionalization process doesn't affect the structure and the crystallinity of the hosting framework.

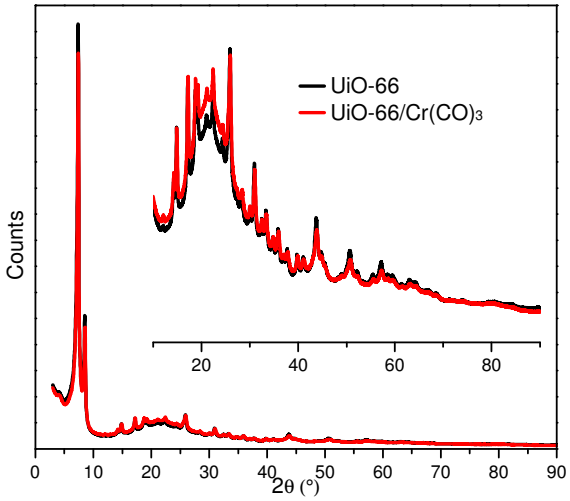

Figure S1. XRPD data (collected in controlled atmosphere) of UiO-66 (dehydrated at 150°C) and of UiO-66/$Cr(CO)_3$.

Few details on the EXAFS data analysis

Phase and amplitudes have been calculated by FEFF6.0 code[Ankudinov, 1998 #60] using as input the structures of (η^6-C_6H_6)$Cr(CO)_3$ and $Cr(CO)_6$ as determined by XRD. For each sample, the averaged $k^3\chi(k)$ function was Fourier transformed in the Δk = 2.0-11.0 $Å^{-1}$ interval. The fits were performed in R-space in the ΔR = 1.1-3.2 Å range (number of independent points $2\Delta k\Delta R/\pi > 12$).

In the EXAFS data analysis of the $Cr(CO)_6$ and (η^6-C_6H_6)$Cr(CO)_3$ reference samples, the following signals have been considered: (i) the Cr-C single scattering (SS) paths (with degeneration 6 and 3, respectively); (ii) the Cr-O SS paths (with degeneration 6 and 3, respectively); (iii) the collinear MS paths involving the C and O atoms of the carbonyl ligands (with degeneration 18 and 6, respectively); (iv) in the case of (η^6-C_6H_6)$Cr(CO)_3$ also the SS Cr-C paths involving the benzene rings (degeneration 6) have been considered, whereas the corresponding MS paths were estimated to be negligible. In both cases, the CO molecule was considered as a rigid unit at a C-O distance of 1.15 Å, as resulting from the XRD structures. In this way, only 4 parameters have been optimized in the case of $Cr(CO)_6$ (see first column in Table 1, main text): S_0^2 and ΔE_0 (common to all paths), the Cr-CO distance $R_{Cr\text{-}CO}$, and an unique Cr-CO Debye-Waller factor for the SS paths (σ^2_{CO}), that propagates to the MS paths according to the square of the path length. In the case of (η^6-C_6H_6)$Cr(CO)_3$, two additional parameters have been considered (see second column in Table 1, main text): the distance between Cr and C atoms of the benzene ring ($R_{Cr\text{-}Bz}$) and the corresponding Debye-Waller factor (σ^2_{Bz}). Finally, the S_0^2 value optimized for the (η^6-C_6H_6)$Cr(CO)_3$ model system was kept fixed in the fit of the PS/$Cr(CO)_3$ sample, whereas the number of CO and C ligands were allowed to change.

Spectroscopic evidences of formation of (arene)Mo(CO)$_3$ complex

Vibrational properties: in situ FT-IR spectroscopy

The FT-IR spectra of $Mo(CO)_6$ adsorbed on PS and UiO-66, shown in Figure S2, As previously observed in case of $Cr(CO)_6$ in the same matrices, the $Mo(CO)_6$ symmetry is slightly distorted with respect to that of the molecule in the gas phase. This is evedenced by the presence, together with the dominant (out of scale) IR absorption band centered around 1980 cm^{-1} (IR-active mode), of weaker absorption bands at higher frequency (2012 and 2019 cm^{-1} in UiO-66 and PS, respectively), which can be assigned to the E_g vibrational mode (IR inactive). As for $Cr(CO)_6$, also $Mo(CO)_6$ is irreversibly adsorbed in UiO-66, while in PS it can be removed easily by pumping at RT. Therefore, the same strategy has been followed to thermally decompose the $Mo(CO)_6$ precursor. After the thermal decomposition of $Mo(CO)_6$, the IR spectra are characterized by two new absorption bands, at 1966 and 1891 cm^{-1} in the case of PS, and at 2001 and 1943 cm^{-1} in the case of UiO-66. The resulting spectra, very similar to those observed in the case of functionalization with $Cr(CO)_3$ unities, testify the grafting of $Mo(CO)_3$ species to the benzene rings of the supporting matrices. As already discussed in the case of $Cr(CO)_3$, also in the present case the IR spectrum of UiO-66/$Mo(CO)_3$ shows a more complex structure with respect to that of PS/$Mo(CO)_3$, with additional components at 1915 cm^{-1} (shoulder) and at 1895 cm^{-1}. This observation can be explained by considering that the $Mo(CO)_3$ moieties in UiO-66 feel a slightly different environment, depending on the type of cage where they are (the smaller tetrahedral or the larger hexahedral).

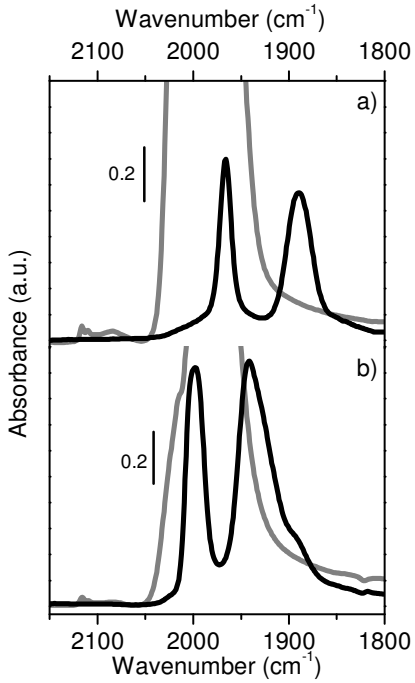

Figure S2. FTIR spectra of $Mo(CO)_6$ (dark grey) and (η^6-C_6H_6)$Mo(CO)_3$ in PS and UiO-66 supports (top and bottom partsarts a and b, respectively), in the ν(CO) region.

The stability of the grafted $Mo(CO)_3$ species was monitored in presence of CO (by adding 40 mbar of CO in a closed cell at room temperature) and of moisture (by opening the cell at ambient atmosphere). The results are reported in Figure S3. As already observed in the case of the $Cr(CO)_3$ complexes, the species grafted in PS matrix are more stable than that grafted in UiO-66, both in presence of CO and of moisture; however, in both matrices, the $Mo(CO)_3$ species are less stable

than the parent $Cr(CO)_3$ ones. A small fraction of $Mo(CO)_6$ is formed in both matrices in presence of CO (following the reverse reaction (arene)$Mo(CO)_3$ + CO = $Mo(CO)_6$ + arene), as testified by the growth of a band at 1984 cm^{-1}. When exposed to air, the PS/$Mo(CO)_3$ system shows a very slow decomposition, whereas almost all the UiO-66/$Mo(CO)_3$ complexes are destroyed. This behavior, even if less pronounced, was already reported in the cse of the (arene)$Cr(CO)_3$ systems, and explained by considering the higher hydrophylicity of the UiO-66 matrix with respect to the PS one.

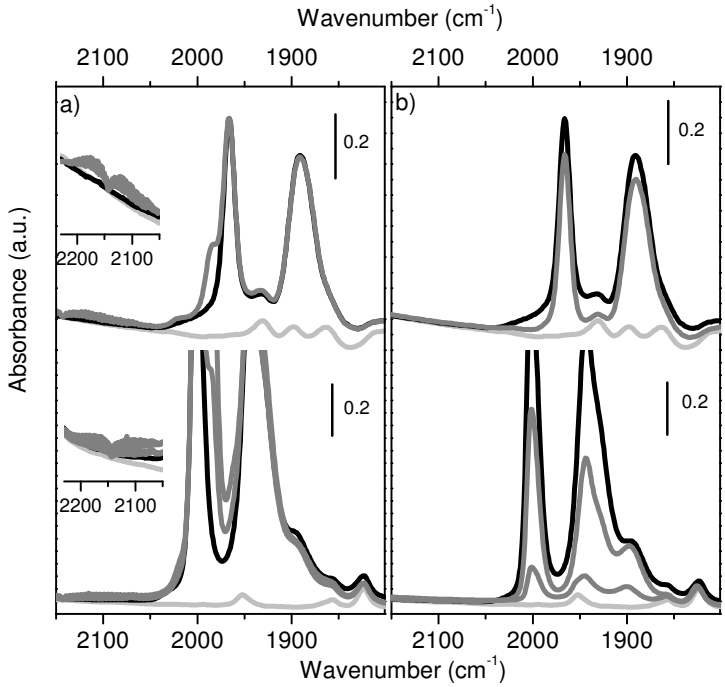

Figure S3. Reversibility in presence of CO (part a) and stability in air (part b) of (arene)$Mo(CO)_3$ species formed in PS (top) and UiO-66 (bottom). Light grey: backgorund; Black: (arene)$Mo(CO)_3$, Grey: evolution upon CO dosage or exposure to air. Inset in part a shows the frequency region 2250-2030 cm^{-1}, where rotovibrational features of gaseous CO is present

Optical properties: in situ DR UV-Vis-NIR spectroscopy

Upon heating the PS and UiO-66 matrices in presence of $Mo(CO)_6$ the samples became colored, pale and dark orange in the two cases, respectively. The corresponding diffuse reflectance spectra, shown in Figure S4, are very similar to those obtained for PS and UiO-66 functionalized with $Cr(CO)_3$, with only minor variation in the band frequency.

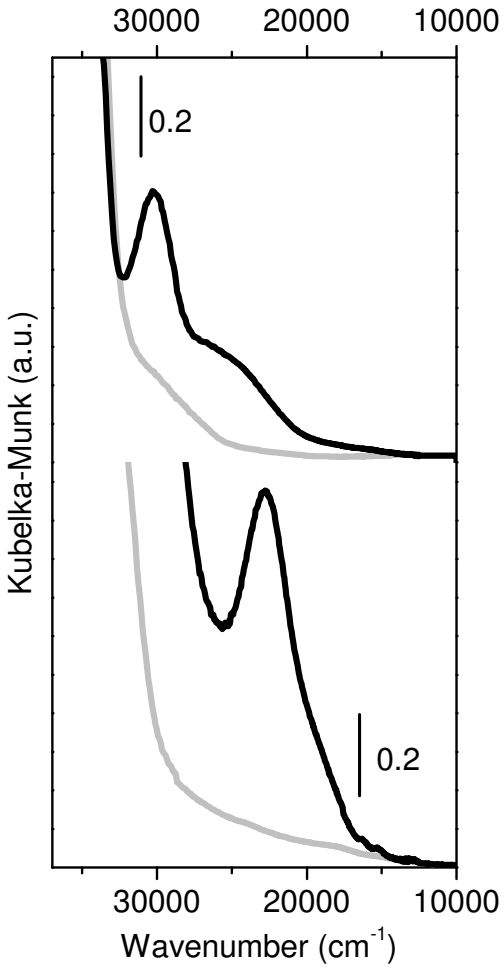

Figure S4. UV-Vis DRS spectra of activated matrix (grey) and (arene)$Mo(CO)_3$ complex (black) inside PS (top part) and UiO-66 (bottom part).